

## Phonon dispersion of graphite by inelastic x-ray scattering

M. Mohr,<sup>1,\*</sup> J. Maultzsch,<sup>1,†</sup> E. Dobardžić,<sup>2</sup> S. Reich,<sup>3</sup> I. Milošević,<sup>2</sup> M. Damnjanović,<sup>2</sup> A. Bosak,<sup>4</sup> M. Krisch,<sup>4</sup> and C. Thomsen<sup>1</sup><sup>1</sup>*Institut für Festkörperphysik, Technische Universität Berlin, Hardenbergstrasse 36, 10623 Berlin, Germany*<sup>2</sup>*Faculty of Physics, University of Belgrade, POB 368, 11011 Belgrade, Serbia*<sup>3</sup>*Department of Materials Science and Engineering, Massachusetts Institute of Technology, 77 Massachusetts Avenue, Cambridge, Massachusetts 02139-4307, USA*<sup>4</sup>*European Synchrotron Radiation Facility (ESRF), BP 220, F-38043 Grenoble Cedex, France*

(Received 20 March 2007; revised manuscript received 27 April 2007; published 30 July 2007)

We present the full in-plane phonon dispersion of graphite obtained from inelastic x-ray scattering, including the optical and acoustic branches, as well as the midfrequency range between the  $K$  and  $M$  points in the Brillouin zone, where the experimental data have been unavailable so far. The existence of a Kohn anomaly at the  $K$  point is further supported. We fit a fifth-nearest neighbor force-constant model to the experimental data, making improved force-constant calculations of the phonon dispersion in both graphite and carbon nanotubes available.

DOI: 10.1103/PhysRevB.76.035439

PACS number(s): 81.05.Uw, 63.20.Dj, 63.70.+h, 78.70.Ck

## I. INTRODUCTION

Research on carbon nanotubes and the recent availability of single graphite sheets<sup>1,2</sup> (graphene) have revived the interest in the fundamental physical properties of graphite during the past years. Carbon nanotubes can be regarded as one or more rolled-up graphite sheets, and many physical properties of carbon nanotubes are closely related to those of graphite.<sup>3,4</sup>

The fundamental characteristics of a crystalline material comprise its phonon spectrum, from which one can derive several other physical properties, such as sound velocity, thermal conductivity, or heat capacity. Furthermore, phonons play an important role in excited-state dynamics and electrical transport properties. Optical or electronic excitations can decay into vibrational excitations or can be scattered by phonons into different states. For example, in carbon nanotubes, the high-bias electrical transport is assumed to be limited by scattering of the carriers by optical phonons corresponding to the graphite  $K$  point.<sup>5,6</sup>

The phonon dispersion of graphite has not been completely resolved by experiment, mostly due to the lack of large enough samples of crystalline quality. It has been partly measured by inelastic neutron scattering (INS), electron-energy loss spectroscopy (EELS), and inelastic x-ray scattering (IXS).<sup>7-11</sup> Most experiments so far have determined the dispersion along the  $\Gamma$ - $K$  and the  $\Gamma$ - $M$  directions in the graphite Brillouin zone (see Fig. 1 for a definition of the Brillouin zone). The recent measurement of the optical branches along the  $K$ - $M$  direction by IXS pointed to the existence of a Kohn anomaly for the highest phonon branch at the  $K$  point.<sup>11,12</sup> Although this result resolved previous discrepancies between different lattice dynamics models, there are still open questions regarding the shape of lower-lying phonon branches. In particular, differences appear between force-constant and density-functional theory (DFT) calculations, where experimental data are still unavailable. This concerns, e.g., the crossing between the acoustic and optical bands near the  $M$  point or the energy of the transverse acous-

tic mode at the  $K$  point. For carbon nanotubes, the experimental determination of the phonon dispersion throughout the entire Brillouin zone would require monocrystalline samples of a minimum size, which have been unavailable so far. Therefore, the closest approximation to the experimental phonon dispersion of carbon nanotubes is currently the phonon dispersion of graphite.

Here, we present the phonon dispersion of graphite in all three high-symmetry directions in the basal plane determined by inelastic x-ray scattering. In particular, the phonon branches between the  $K$  and  $M$  points and the acoustic branches in all high-symmetry directions are obtained, giving both the optical and acoustic phonons from one experimental technique. We fit our data by a set of force constants, including the fifth-nearest neighbors of carbon atoms. The fitted force constants can be used to deduce the corresponding force constants for carbon nanotubes.

This paper is organized as follows. In the next section, we briefly describe the experimental details of the IXS experiments. We give an introduction to the phonon dispersion of graphite and present the experimental data in Sec. III. In Sec. IV, we apply a fifth-nearest neighbor force-constant fit to the experimental data and provide the in-plane and out-of-plane force constants.

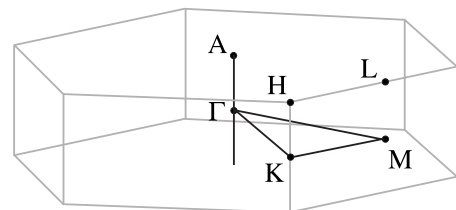


FIG. 1. Brillouin zone of graphite. The Brillouin zone of graphene is the hexagon which lies in the plane with the points  $\Gamma$ ,  $K$ , and  $M$ . The distances between the high-symmetry points are  $\Gamma$ - $K$  =  $4\pi/3a$ ,  $\Gamma$ - $M$  =  $2\pi/\sqrt{3}a$ , and  $K$ - $M$  =  $2\pi/3a$ .

## II. EXPERIMENTAL SETUP

The inelastic x-ray experiments were performed at beamline ID28 at the European Synchrotron Radiation Facility (ESRF). For a review of IXS, the reader is referred to Refs. 13 and 14. The energy of the incident radiation of 17 794 eV was selected by the (999) Bragg reflection of a silicon crystal. The scattered photons were analyzed by five analyzers operating in the same reflection order. The total energy resolution in this configuration is 3.0 meV.<sup>14</sup> The x-ray beam was focused to  $250 \times 60 \mu\text{m}^2$ , selecting a single microcrystal in a naturally grown graphite flake. The typical size of a single grain was about  $800 \mu\text{m}$  in lateral direction and  $100 \mu\text{m}$  along the  $c$  axis. By x-ray diffraction, we obtained the lattice parameters  $a=2.463 \text{ \AA}$  and  $c=6.712 \text{ \AA}$ , in excellent agreement with previous neutron diffraction data ( $a=2.464 \text{ \AA}$ ,  $c=6.711 \text{ \AA}$ ).<sup>15</sup>

Inelastic scattering spectra were recorded by varying the temperature difference between the monochromator and the analyzer silicon crystal. To minimize the effects of temperature drifts that could result in an energy offset, we performed systematic Stokes–anti-Stokes scans between the measurements. In our setup, the  $c$  axis of graphite and the scattering plane encompass angles of  $90^\circ$ ,  $30^\circ$ , and  $0^\circ$ , depending on the phonon branch under consideration. The scattering geometry was chosen according to the selection rules, see Ref. 16.

## III. EXPERIMENTAL RESULTS

The unit cell of graphene contains two atoms, resulting in six phonon branches. The unit cell of graphite consists of four atoms, which leads to 12 phonon branches. The space group of graphite is  $P6_3/mmc$  (international notation). At the  $\Gamma$  point, it possesses the factor group  $6/mmm$  ( $D_{6h}$  in Schönflies notation). The optical zone-center modes of graphene are decomposed into  $\Gamma=B_{2g}+E_{2g}$ . In graphite, the optical zone-center modes are decomposed into  $\Gamma=A_{2u}+2B_{2g}+E_{1u}+2E_{2g}$ .<sup>17–19</sup> The  $A_{2u}$  and  $E_{1u}$  modes are IR active, and the  $E_{2g}$  modes Raman active. The  $B_{2g}$  modes are optically inactive, but can be measured via INS or IXS. The three acoustic modes are decomposed into  $\Gamma=A_{2u}+E_{1u}$ .

Graphite is a highly anisotropic material: the nearest-neighbor distance between the two atoms in the plane is  $a/\sqrt{3} \approx 1.42 \text{ \AA}$ , while the interlayer distance is  $c/2 \approx 3.35 \text{ \AA}$ . The bonds between the two carbon atoms in the plane are much stronger than the weak van der Waals interactions between the layers. Therefore, compared to graphene, one expects that the phonon modes of graphite correspond approximately to in-phase and out-of-phase vibrations of the two graphene planes. Most of the phonon branches in graphite are nearly doubly degenerate and almost the same as in graphene.<sup>12,20</sup> Only close to the  $\Gamma$  point, the acoustic modes of the single layer split in graphite into an acoustic mode (in-phase vibration of the graphene sheets) and an optical mode [out-of-phase vibration; in plane,  $E_{2g}$  at 5.2 meV ( $42 \text{ cm}^{-1}$ ); out of plane,  $B_{2g}$  at 15.7 meV ( $127 \text{ cm}^{-1}$ )]. For the optical modes of graphite, the difference between the in-phase and the out-of-phase vibrations is very small: at the  $\Gamma$  point, the IR active  $E_{1u}$  mode is found at 196.9 meV

( $1588 \text{ cm}^{-1}$ ), close to the Raman active  $E_{2g}$  mode at 196.0 meV ( $1581 \text{ cm}^{-1}$ ). The same holds for the  $A_{2u}$  mode at 107.5 meV ( $867 \text{ cm}^{-1}$ ) (Refs. 17 and 21) and the  $B_{2g}$  mode at 107.6 meV ( $868 \text{ cm}^{-1}$ ). Therefore, in the following theoretical discussion, we will consider the phonons of a single graphene sheet.

The six branches are divided into the out-of-plane acoustic mode ZA, the in-plane acoustic mode TA (sometimes called SH=shear), the longitudinal acoustic mode LA, the out-of-plane optical mode ZO, the in-plane optical mode TO (SH\*), and the longitudinal optical mode LO. Four branches belong to modes where the atoms move in plane with the graphene layer (TA, LA, TO, LO); two branches belong to transverse modes, where the atoms move out of the plane (ZA, ZO).

In Fig. 2, we show our experimental data of the graphite phonon dispersion in the plane. The lines show the fifth-nearest neighbor force-constant fit described in Sec. IV. The optical phonon frequencies near the  $\Gamma$  point agree well with previous experiments. We find the  $E_{2g}$  LO mode at 196.0 meV ( $1581 \text{ cm}^{-1}$ ) and the  $B_{2g}$  mode at 107.6 meV ( $868 \text{ cm}^{-1}$ ). Regarding the overall shape of the phonon branches, our experiments confirm previous *ab initio* DFT calculations, letting aside the special situation for the highest branch at the  $K$  point.<sup>11,12,20,22,23</sup>

As can be seen, the highest optical frequency does not appear at the  $\Gamma$  point. Instead, the phonon frequency first increases with larger wave vector and then decreases again. This effect, called overbending, has been observed in diamond as well.<sup>24</sup> In graphite, it has been predicted to result from a Kohn anomaly, i.e., the frequency at the  $\Gamma$  point is lowered due to interaction of the phonon with the electronic system.<sup>11,12</sup> Another Kohn anomaly in graphite can be found for the TO-derived phonon branch at the  $K$  point [fully symmetric  $A'_1$  ( $K_1$ ) mode]. We have gained additional data for the highest optical phonons around the  $K$  point, confirming previous measurements of the frequency softening of the TO-derived branch near the  $K$  point.<sup>11</sup> Again, we were not able to detect the  $A'_1$  phonon directly at the  $K$  point. The strong electron-phonon interaction has been predicted to reduce the phonon lifetime which results in a line broadening. Probably, the large linewidth makes it very difficult to detect the  $A'_1$  phonon at the  $K$  point experimentally.

Considering the differences between previous theoretical models, we find the following results, see also Sec. IV. Between the  $\Gamma$  and  $M$  points, the ZO and TA modes do not cross within our experimental error of 3 meV. This is in contrast to the previous empirical force-constant models and EELS data of Ref. 8. Which branch is higher directly at the  $M$  point cannot be uniquely distinguished from our data. However, in DFT phonon calculations, the crossing is found between  $K$  and  $M$  but close to  $M$  (about 1/10 of the distance between  $K$  and  $M$ , see Ref. 23). The overall agreement with DFT calculations supports the crossing between  $K$  and  $M$ , see also Fig. 3.

The TA branch along  $\Gamma$ - $M$  shows a smaller increase compared to the EELS data in Ref. 8. In a recent EELS experiment on epitaxially grown thin graphene sheets,<sup>10</sup> however, this branch could not be detected, as the shear modes in

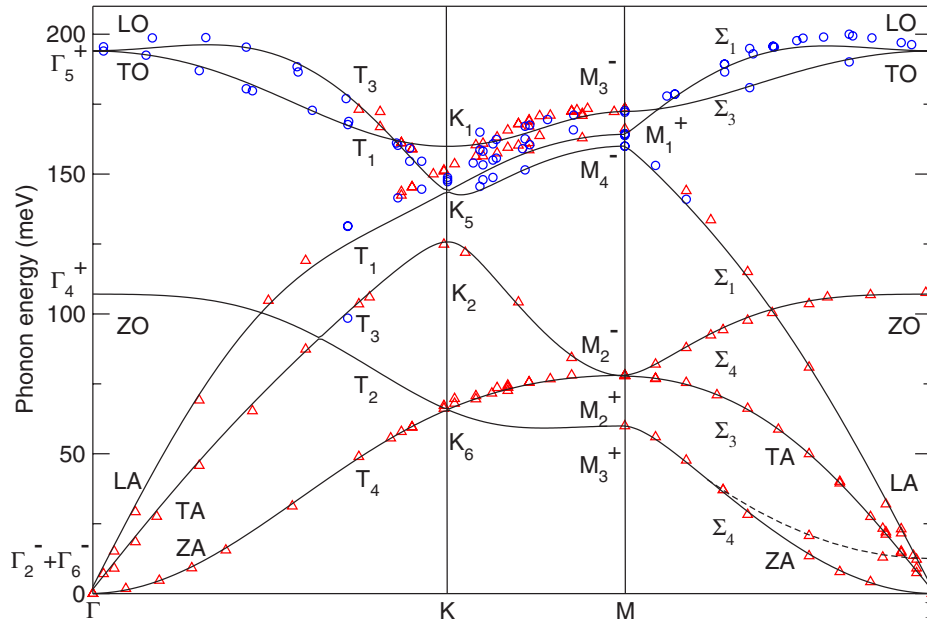


FIG. 2. (Color online) Phonon dispersion of graphite from inelastic x-ray scattering (symbols). Triangles are present data, and circles are data already published in Ref. 11. The full square at the  $\Gamma$  point is INS data from Ref. 7. Solid lines are the force-constant calculations from the fifth-nearest neighbor fit discussed in Sec. IV; the dashed line is a quadratic extrapolation of the data. The lines are denoted by their symmetry representation in space group notation. The relation between space group and molecular notation can be found in Table I.

graphene are forbidden in EELS. These contrasting results suggest that the crystalline quality of Ref. 8 was lower, softening the selection rules. This explains why some previous empirical models, relying on the then available EELS data, predicted a larger slope and consequently a crossing of the ZO and TA modes between the  $\Gamma$  and  $M$  points.

We measured the ZA and TA modes between the  $K$  and  $M$  points, where experimental data of these branches have not been available until now. Our results confirm predictions made by *ab initio* calculations very well (Fig. 3), and are also well reproduced by our force-constant fit (Fig. 2). The trend of both branches crossing near the  $M$  point can be recognized.

The two optical phonons at the  $M$  point derived from the LO and LA branches are very close in frequency

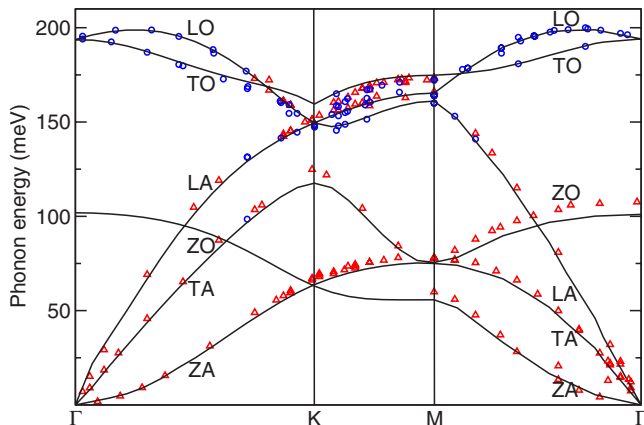


FIG. 3. (Color online) Our in-plane phonon dispersion of graphite together with a DFT calculation from Ref. 11 (solid lines). Same symbols as in Fig. 2 were used.

(<4 meV), and we were not able to distinguish them clearly by symmetry. It appears, however, consistent with DFT calculations and the force-constant fit in Sec. IV that the higher frequency has  $M_1^+$  symmetry and the lower one  $M_4^-$ . As a consequence, the LO- and LA-derived branches cannot cross between the  $K$  and  $M$  points.

In Fig. 4, we show the low-frequency phonon range along the  $\Gamma$ -A direction, i.e., perpendicular to the in-plane direction. For comparison, we also present the INS data on highly oriented pyrolytic graphite from Ref. 7. They are in excellent agreement. The high-frequency phonon range is expected to show almost no dispersion along the  $\Gamma$ -A direction.<sup>20</sup>

We did not measure data points from the ZO branch along the  $\Gamma$ -K-M direction. This branch has been measured in recent EELS experiments of Ref. 10. In general, the data of Ref. 10 agree well with ours, but at the  $K$  point the ZO and ZA branches in Ref. 10 show a relatively large splitting of  $\approx 10$  meV. They cannot stem from the degenerate  $K_6$  pho-

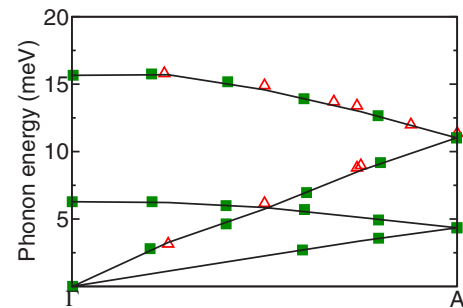


FIG. 4. (Color online) Phonon dispersion of graphite along the  $\Gamma$ -A direction. Open triangles are present IXS data, and full squares are neutron scattering data from Ref. 7. The lines are a guide to the eye.

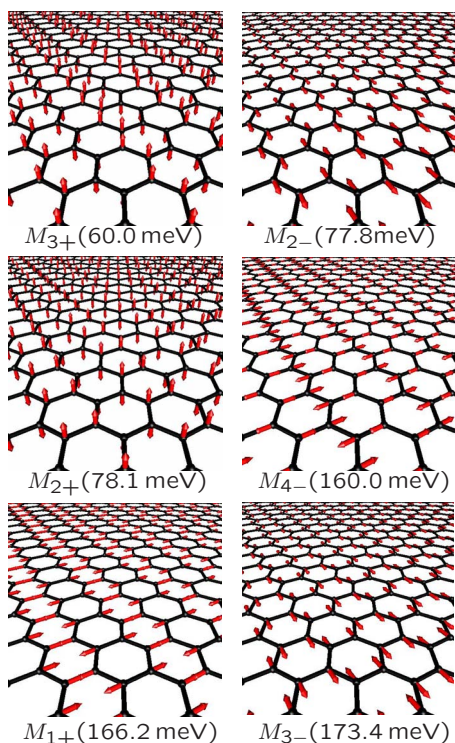


FIG. 5. (Color online) Eigenmodes of graphene at the  $M$  point (from lower to higher frequencies). Phonon energies given in parentheses are the IXS experimental values. For the symmetry notation, see Table I.

non, but could possibly represent the out-of-phase modes of the graphite planes. On the other hand, in DFT calculations of graphite,<sup>20</sup> this splitting seems much smaller than indicated by the EELS data.

Regarding the phonon modes specific for graphite with more than one layer, we observe the low-energy out-of-phase modes near the  $\Gamma$  point. These are indicated by the dashed line in Fig. 2. We measured two out-of-phase ZO' phonons in the  $\Gamma$ - $M$  direction, with energies 13.6 and 23.3 meV at 0.16 of the  $\Gamma$ - $M$  distance and at  $0.4\Gamma$ - $M$ , respectively. A quadratic extrapolation leads to a value of 12.5 meV at the  $\Gamma$  point, in agreement with 15.7 meV from neutron scattering data.<sup>7</sup>

The optical-phonon frequencies at the high-symmetry points from our experiment are summarized in Figs. 5–7 together with the displacement patterns obtained by the force-

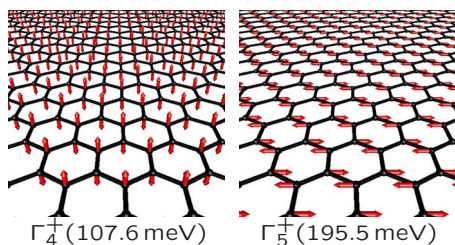


FIG. 6. (Color online) Optical eigenmodes of graphene at the  $\Gamma$  point from the force-constant calculation. The experimental frequency values are given in parentheses; they are taken from the data recorded closest to the  $\Gamma$  point.

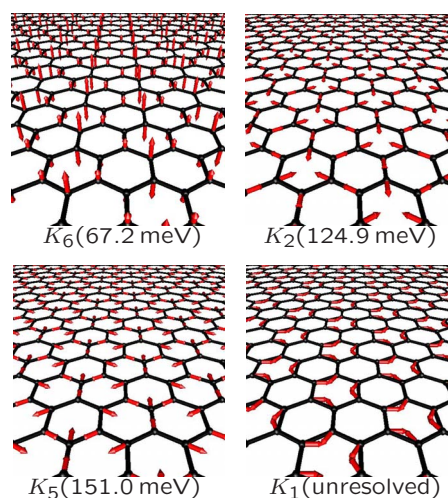


FIG. 7. (Color online) Eigenmodes of graphene at the  $K$  point. For the degenerate modes, only one choice per energy is given. Phonon energies given in parentheses are the IXS experimental values. For the symmetry notation, see Table I.

constant calculations in Sec. IV. The acoustic phonon branches near the  $\Gamma$  point give information on the elasticity of graphite, which will be reported elsewhere.<sup>25</sup>

#### IV. FORCE-CONSTANT CALCULATIONS

Phonon dispersion relations are often predicted from *ab initio* DFT or from empirical force-constant (FC) calculations. Empirical force-constant models in graphite have so far included up to fourth-nearest neighbors, in order to reproduce the overbending of the optical branch near the  $\Gamma$  point.<sup>26,27</sup> In the case of graphite, besides the details regarding the frequency values, both methods show differences in the shape of phonon branches, e.g., the position of the crossing of the ZO and TA modes near the  $M$  point. While in FC calculations, a crossing of the ZO and TA branches between the  $\Gamma$  and  $M$  points is predicted; it is found in *ab initio* results to take place between  $K$  and  $M$ . This probably stems from a fit to the only available TA mode from EELS experiments in Ref. 8, as our force-constant fit will show later (e.g., see Ref. 27).

Further differences between force-constant and *ab-initio* DFT calculations are found regarding the LA and LO branches near the  $M$  point: In DFT results, the LO-derived phonon branch is higher than the LA phonon at the  $M$  point, and, as a result, the two branches do not cross between  $M$  and  $K$ , vice versa in most predictions by empirical force constants.

Discrepancies with the experimental data are found for both models for the TO-derived branch at the  $K$  point, except for Ref. 28. In this context, we want to emphasize the importance of the  $K$  point, when performing DFT calculations. The atomic forces in graphite are long ranged. Therefore, when using the finite-difference approach and DFT,<sup>11,22,23</sup> only the phonons commensurate with the supercell are calculated correctly. In linear-response calculations, on the other hand, the implementation of the  $K$  point can be more easily

TABLE I. Symmetry relations between space group and molecular notation for the space group  $P6_3/mmc$  and the point group  $D_{6h}$ . The corresponding coordinate system for  $C_{2v}$  is shown in Fig. 8.

$\Gamma$	$D_{6h}$	$K$	$D_{3h}$	$M$	$D_{2h}$	$T, \Sigma$	$C_{2v}$
$\Gamma_2^-$	$A_{2u}$	$K_1$	$A_1'$	$M_1^+$	$A_{1g}$	$T_1, \Sigma_1$	$A_1$
$\Gamma_4^+$	$B_{2g}$	$K_2$	$A_2'$	$M_2^+$	$B_{1g}$	$T_2, \Sigma_2$	$A_2$
$\Gamma_6^-$	$E_{1u}$	$K_5$	$E'$	$M_2^-$	$B_{1u}$	$T_3, \Sigma_3$	$B_1$
$\Gamma_5^+$	$E_{2g}$	$K_6$	$E''$	$M_3^+$	$B_{2g}$	$T_4, \Sigma_4$	$B_2$
				$M_3^-$	$B_{2u}$		
				$M_4^-$	$B_{3u}$		

achieved;<sup>12,20</sup> however, the dynamical matrix at the  $K$  point should be explicitly calculated and not be simply interpolated.

### A. Fitting procedure

To obtain the optimal fit of the set of force constants to the experimental data, we applied a variable neighbor search method of global optimization,<sup>29</sup> using the simplex method<sup>30</sup> for the local optimization subroutine. Basically, this is the least squares procedure minimizing the average deviation  $\Delta(\mathbf{f}) = \frac{1}{N^{\text{expt}}} \sqrt{\sum_i |\omega_i^{\text{expt}} - \omega_i(\mathbf{f})|^2}$  between the  $N^{\text{expt}}=96$  experimental values  $\omega_i^{\text{expt}}$  and the corresponding calculated frequencies  $\omega_i(\mathbf{f})$  obtained by calculation with the trial values of the force constants  $\mathbf{f}=(f_1, \dots, f_F)$ . Due to symmetry, for each level of the three or six neighbor atoms, the same triple of force constants can be used. We used stretching, out-of-plane, and in-plane force constants  $f_i$  for each relevant pair of atoms.<sup>27,31</sup> Here, the direction of stretching corresponds to the line that connects the center atom with the atom of appropriate level. The in-plane and out-of-plane directions are perpendicular to this line and lie in the graphene layer or perpendicular to it, respectively. After transforming the stretching and in-plane force constants to a global basis, one obtains the dynamical matrix. The level of the relevant neighbors has been gradually increased until the satisfactory agreement ( $\Delta < 0.23$  meV, with the greatest difference of  $|\omega_i^{\text{expt}} - \omega_i(\mathbf{f})| \approx 8$  meV for the LA branch in the  $\Gamma$ - $K$  region, nearby the  $K$  point) has been eventually achieved with included neighbors of up to the fifth level. The fifth level contains 24 neighbors of each atom, as there are 3, 6, 3, 6, and 6 symmetrically positioned first to fifth neighbors, respectively, resulting in 15 independent variational parameters  $f_i$ .

### B. Force-constant results

The optimized values of the force-constant parameters are presented in Table II. In Fig. 2, we show the phonon dispersion obtained from these force constants in comparison with the experimental data. The largest deviations between the calculation and the experiment occur for the optical phonon branches near the  $K$  point. This is probably due to the strong interaction of the near- $K$ -point phonons with electrons near the Fermi level, which is not included in a force-constant model. Including more than fourth-nearest neighbors of atoms (i.e., 15 independent parameters), however, gives a

fairly good description of the local minimum of the TO-derived branch at the  $K$  point.

Moreover, although FC calculations including only fourth-nearest neighbors provide a considerably good average fit to the experimental data, they lead to permuted frequencies of the LO- and LA-derived phonons at the  $M$  point ( $M_1^+$  and  $M_4^-$ ), and to a crossing of the LA and LO branches within the  $K$ - $M$  region ( $K_5$ - $M_1^+$  and  $K_5$ - $M_4^-$ ). Therefore, at least fifth-nearest neighbors are required for a good empirical description of the graphite phonon dispersion.

The eigenvectors of all optical phonons from our force-constant calculation at the high-symmetry points  $\Gamma$ ,  $K$ , and  $M$  are drawn in Figs. 5–7, respectively. They are in agreement with calculations from a molecular-based approach of Ref. 28. For the degenerate modes, we show only one choice per energy; the remaining eigenvectors can be obtained by the symmetry-group projectors.

Often in literature, the molecular notation for the symmetry groups is used. Therefore, Table I shows the relation between the space group notation of  $P6_3/mmc$  and the molecular notation at the high-symmetry points  $\Gamma$ ,  $K$ , and  $M$ , and the lines  $\Gamma$ - $K$ - $M$  ( $T$ ) and  $\Gamma$ - $M$  ( $\Sigma$ ). Figure 8 shows a definition of the coordinate system for the  $C_{2v}$  point group. The eigenvectors will help to choose the sample orientation in future IXS experiments. The scattering cross section is zero, if the direction of the atomic displacements and the momentum transfer in the scattering process enclose an angle of  $90^\circ$ .

The above force-constant parameters can, in principle, be used to calculate the phonon dispersion of carbon nanotubes, in particular, for chiral nanotubes with a large number of atoms in the unit cell that require large computational effort, when calculated with first-principles methods. The existence of a fourth acoustic mode (pure rotation of the tube about its axis) and the finite frequency of the radial breathing mode

 TABLE II. Force-constant parameters for graphene, obtained from a fit to the experimental data, in eV/Å<sup>2</sup>.

Neighbor level	Stretching	Out of plane	In plane
1	25.880	6.183	8.420
2	4.037	-0.492	-3.044
3	-3.016	0.516	3.948
4	0.564	-0.521	0.129
5	1.035	0.110	0.166

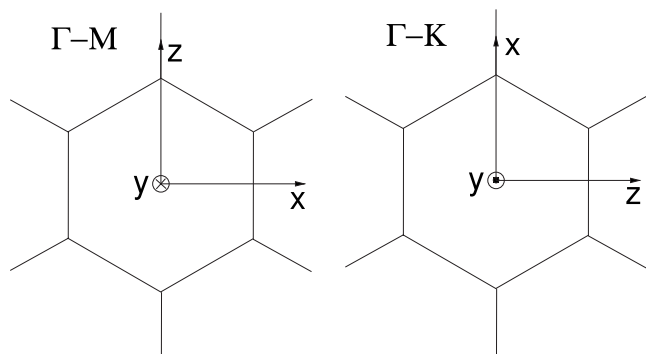


FIG. 8. Coordinate system for the point group  $C_{2v}$  of  $\Gamma$ - $M$  and  $\Gamma$ - $K$  drawn in real space.  $z$  points in the direction of the principal rotational axis.

have to be taken into account, see Refs. 31–33. In addition, the different bond angles and lengths between the carbon atoms on the cylinder surface depending on the chiral index must be included. We expect that such an approach based on the empirical force constants of graphite will give an overall good description of the phonon bands of carbon nanotubes. In metallic nanotubes, however, the coupling of the  $\Gamma$ -point and  $K$ -point phonons to the electronic system will lead to different results for those modes, see, for instance, the Kohn anomalies and the frequency drop of the LO phonon in metallic nanotubes.<sup>12,23,34</sup> Therefore, where the phonon disper-

sion is modified due to the strong interactions between the phonons and the electrons, a force-constant model might only give an empirical description of the phonon bands, but should be tested by DFT calculations which take electron-phonon coupling into account.

## V. SUMMARY

In summary, we presented the full in-plane phonon dispersion of graphite determined by inelastic x-ray scattering. The overall shape of the phonon bands confirms previous *ab initio* DFT calculations, if special care is taken for the highest optical phonons near the  $K$  point. We showed that by including fifth-nearest neighbors, the phonon bands can be well described within a force-constant model. Previous empirical models predicted only parts of the phonon dispersion correctly, since experimental data in the  $K$ - $M$  region had been missing. The force constants will also improve the models of the phonon dispersion in carbon nanotubes.

## ACKNOWLEDGMENTS

We would like to thank M. Dražić for sharing his results prior to publication. We thank A. V. Tamashauskyy for the rare single crystals of graphite. J. M. acknowledges support from the Alexander-von-Humboldt foundation. This work was supported in part by the ESRF.

\*marcel@physik.tu-berlin.de

<sup>†</sup>Present address: Departments of Electrical Engineering and Physics, Columbia University, New York, NY 10027, USA.

<sup>1</sup>K. S. Novoselov, A. K. Geim, S. V. Morozov, D. Jiang, Y. Zhang, S. V. Dubonos, I. V. Grigorieva, and A. A. Firsov, *Science* **306**, 666 (2004).

<sup>2</sup>Y. Zhang, Y.-W. Tan, H. L. Stormer, and P. Kim, *Nature (London)* **438**, 201 (2005).

<sup>3</sup>S. Reich, C. Thomsen, and J. Maultzsch, *Carbon Nanotubes: Basic Concepts and Physical Properties* (Wiley-VCH, Berlin, 2004).

<sup>4</sup>C. Thomsen and S. Reich, in *Light Scattering in Solids IX*, Topics in Applied Physics Vol. 108, edited by M. Cardona and R. Merlin (Springer, Heidelberg, 2007), Chap. 3.

<sup>5</sup>J.-Y. Park, S. Rosenblatt, Y. Yaish, V. Sazanava, H. Üstünel, S. Braig, T. A. Arias, P. W. Brouwer, and P. L. McEuen, *Nano Lett.* **4**, 517 (2004).

<sup>6</sup>M. Lazzeri and F. Mauri, *Phys. Rev. B* **73**, 165419 (2006).

<sup>7</sup>R. Nicklow, N. Wakabayashi, and H. G. Smith, *Phys. Rev. B* **5**, 4951 (1972).

<sup>8</sup>C. Oshima, T. Aizawa, R. Souda, Y. Ishizawa, and Y. Sumiyoshi, *Solid State Commun.* **65**, 1601 (1988).

<sup>9</sup>S. Siebentritt, R. Pues, K.-H. Rieder, and A. M. Shikin, *Phys. Rev. B* **55**, 7927 (1997).

<sup>10</sup>H. Yanagisawa, T. Tanaka, Y. Ishida, M. Matsue, E. Rokuta, S. Otani, and C. Oshima, *Surf. Interface Anal.* **37**, 133 (2005).

<sup>11</sup>J. Maultzsch, S. Reich, C. Thomsen, H. Requardt, and P. Ordejón,

*Phys. Rev. Lett.* **92**, 075501 (2004).

<sup>12</sup>S. Piscanec, M. Lazzeri, F. Mauri, A. C. Ferrari, and J. Robertson, *Phys. Rev. Lett.* **93**, 185503 (2004).

<sup>13</sup>E. Burkel, *Rep. Prog. Phys.* **63**, 171 (2000).

<sup>14</sup>M. Krisch and F. Sette, in *Light Scattering in Solids IX*, Topics in Applied Physics Vol. 108, edited by M. Cardona and R. Merlin (Springer, Berlin, 2007).

<sup>15</sup>P. Trucano and R. Chen, *Nature (London)* **258**, 136 (1975).

<sup>16</sup>A. K. Kirov, M. I. Aroyo, and J. M. Perez-Mato, *J. Appl. Crystallogr.* **36**, 1085 (2003); see also the Bilbao crystallographic server, <http://www.cryst.ehu.es>

<sup>17</sup>R. J. Nemanich and S. A. Solin, *Phys. Rev. B* **20**, 392 (1979).

<sup>18</sup>T. Inui, Y. Tanabe, and Y. Onodera, *Group Theory and its Application in Physics* (Springer, Berlin, 1996).

<sup>19</sup>S. Reich and C. Thomsen, *Philos. Trans. R. Soc. London, Ser. A* **362**, 2271 (2004).

<sup>20</sup>P. Pavone, R. Bauer, K. Karch, O. Schütt, S. Vent, W. Windl, D. Strauch, S. Baroni, and S. de Gironcoli, *Physica B* **219**, 439 (1996).

<sup>21</sup>R. J. Nemanich, G. Lucovsky, and S. A. Solin, *Solid State Commun.* **23**, 117 (1977).

<sup>22</sup>D. Sánchez-Portal, E. Artacho, J. M. Soler, A. Rubio, and P. Ordejón, *Phys. Rev. B* **59**, 12678 (1999).

<sup>23</sup>O. Dubay and G. Kresse, *Phys. Rev. B* **67**, 035401 (2003).

<sup>24</sup>S. Han and J. Ihm, *Phys. Rev. B* **66**, 241402(R) (2002).

<sup>25</sup>A. Bosak, M. Krisch, M. Mohr, J. Maultzsch, and C. Thomsen, *Phys. Rev. B* **75**, 153408 (2007).

- <sup>26</sup>R. Al-Jishi and G. Dresselhaus, *Phys. Rev. B* **26**, 4514 (1982).
- <sup>27</sup>R. A. Jishi, L. Venkataraman, M. S. Dresselhaus, and G. Dresselhaus, *Chem. Phys. Lett.* **209**, 77 (1993).
- <sup>28</sup>C. Mapelli, C. Castiglioni, G. Zerbi, and K. Müllen, *Phys. Rev. B* **60**, 12710 (1999).
- <sup>29</sup>M. Dražić, C. Lavor, N. Maculan, and N. Mladenović, *J. Oper. Res. Soc.* (to be published).
- <sup>30</sup>W. Press, B. P. Flannery, S. A. Teukolsky, and W. T. Vetterling, *Numerical Recipes* (Cambridge University Press, Cambridge, 1986).
- <sup>31</sup>E. Dobardžić, I. Milošević, B. Nikolić, T. Vuković, and M. Damjanović, *Phys. Rev. B* **68**, 045408 (2003).
- <sup>32</sup>R. Saito, T. Takeya, T. Kimura, G. Dresselhaus, and M. S. Dresselhaus, *Phys. Rev. B* **57**, 4145 (1998).
- <sup>33</sup>J. Maultzsch, S. Reich, C. Thomsen, E. Dobardžić, I. Milošević, and M. Damjanović, *Solid State Commun.* **121**, 471 (2002).
- <sup>34</sup>S. Piscanec, M. Lazzeri, J. Robertson, A. C. Ferrari, and F. Mauri, *Phys. Rev. B* **75**, 035427 (2007).